THE JOURNAL OF PHYSICAL CHEMISTRY B

Article

pubs.acs.org/JPCB

Effects of Temperature on the Thermodynamic and Dynamical Properties of Glycerol–Water Mixtures: A Computer Simulation Study of Three Different Force Fields

Frederick O. Akinkunmi, David A. Jahn, and Nicolas Giovambattista*

Department of Physics, Brooklyn College of the City University of New York, Brooklyn, New York 11210, United States

ABSTRACT: Glycerol–water solutions are relevant in technological and scientific applications, such as in the preservation of biomolecules and tissues at low temperatures. We perform molecular dynamics simulations of glycerol–water mixtures with glycerol molar fractions of χ_g = 0–100% at P = 0.1 MPa and T = 210–460 K. We focus on the effects of temperature and concentration on the thermodynamic (density ρ, thermal expansion coefficient α_P, isobaric specific heat c_P, compressibility κ_T) and dynamical (glycerol and water diffusion coefficients, D_g and D_w) properties of the mixtures. In particular, we test the sensitivity of computer simulation results to the glycerol force field and water model (TIP3P and TIP4P/2005) employed. All mixture models underestimate ρ at high T and tend to overestimate ρ at low T; only the mixture model based on TIP4P/2005 water exhibits a density maximum at low χ_g, as expected. All models overestimate α_P, c_P, and κ_T; they are able to reproduce qualitatively the T dependence of α_P and κ_T but fail in the case of c_P. In all cases, D_g and D_w follow the Vogel–Tamman–Fulcher equation and decouple at low T, with D_w/D_g increasing upon cooling. Overall, the mixture based on TIP4P/2005 water provides better thermodynamic and dynamical properties than the mixtures based on TIP3P water, even at χ_g = 20%.

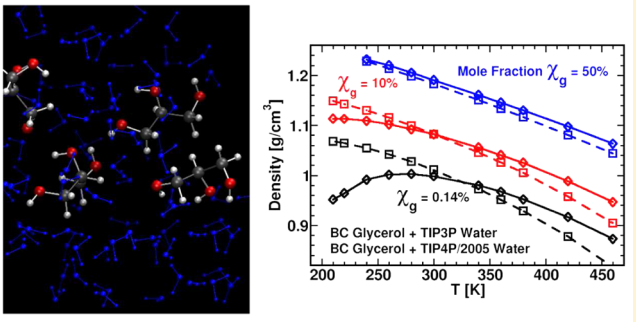

1. INTRODUCTION

Glycerol ($C_3H_8O_3$) is a syrupy, sweet-tasting, colorless, and odorless liquid under normal conditions. It was discovered by Scheele in the late 1700s by mixing olive oil with litharge and heating.[1] (A brief introduction to the early history of glycerol can be found in ref 2.) Since its discovery, the use of glycerol has increased rapidly, and it is currently used in a wide range of applications,[3] from the cryopreservation of cells and tissues[4] to the manufacturing of inks, adhesives, synthetic plastics, and even explosives.[5] Glycerol is commonly used in the pharmaceutical, cosmetics, and food industries, and recent interest in glycerol has been boosted by its potential as a solvent for green chemistry.[6]

The relevance of glycerol in scientific and technical applications has motivated many computational studies involving glycerol and, in particular, water–glycerol mixtures (refs 7–19); computational studies of biomolecules in water–glycerol mixtures are not uncommon (refs 20–23). Not surprisingly, such studies may be sensitive to the glycerol–water mixture model employed, and hence the validation of the water–glycerol FF is a necessary preliminary step for such studies. Unfortunately, the benchmarking of FFs for water–glycerol mixtures (or other binary aqueous solutions) with experimental data is a time-consuming task, and in most studies this is overlooked. If included, benchmarking of the target FF is usually limited to comparing a few properties of the mixture model with experiment, such as density and solvation energy, and it is usually done under only a few thermodynamic conditions (e.g., P = 1 atm and selected concentrations (refs 15, 19, and 24)). The case of water–glycerol mixtures, in contrast to water–ions solutions, is more complex. This is because glycerol is a small flexible molecule that can adopt different molecular conformations (refs 25–27). We note that computational studies of glycerol–water mixtures predict different molecular conformations of glycerol depending on the FF employed (refs 10, 13, and 27). This implies that, from the microscopic point of view, there is evidence suggesting that different water–glycerol mixture models may provide alternative liquid environments. If so, computer simulation results of a guest biomolecule in such solutions may differ qualitatively depending on the water–glycerol mixture model used. From a general point of view, it should be clear that comparing the performance of computational models of glycerol–water mixtures is highly desirable for interpreting experimental studies.[28]

This is the second of a series of computational studies with the goal of investigating the properties of glycerol and glycerol–water mixtures in a wide range of temperatures and concentrations and comparing different computational models. In a previous work, we studied (pure) glycerol employing five

Received: January 15, 2015
Revised: April 21, 2015
Published: April 22, 2015

DOI: 10.1021/acs.jpcb.5b00439
J. Phys. Chem. B 2015, 119, 6250–6261

different FFs. It was found that the FFs studied perform better or worse depending on the properties considered, and hence the best model for glycerol is not evident. In particular, they provide different molecular conformations indicating that, depending on the model considered, glycerol molecules form a different number of inter- and intramolecular hydrogen bonds (HBs). Accordingly, one may also expect a different number of HBs between water and glycerol, depending on the FFs employed. In this work, we choose two of the previously studied glycerol FFs and explore their behavior in the presence of water. Two water models are considered, and we focus on a total of three glycerol−water mixture models. We cover temperatures in the range of 210−460 K and glycerol molar fractions of χ_g = 0−100% at P = 0.1 MPa. One of the main goals of this work is to test whether the addition of water reduces the differences in the properties of pure glycerol FFs as reported in ref 27 and, if so, to identify the minimum concentration at which this occurs. In this work, we report thermodynamic (density ρ, thermal expansion coefficient α_P, isobaric specific heat c_P, and compressibility κ_T) and dynamical (glycerol and water diffusion coefficients, D_g and D_w) properties of each glycerol−water mixture model; the corresponding structural properties (e.g., glycerol conformation, pair correlation functions, etc.) will be reported in a separate work (in preparation).

This work is organized as follows. In section 2, we discuss the computational details and describe the FFs studied. The thermodynamic and dynamical properties of glycerol−water mixtures are presented in sections 3 and 4, respectively. A summary and discussion are included in section 5.

2. COMPUTER SIMULATION DETAILS

We perform molecular dynamics (MD) simulations of water−glycerol mixtures at P = 0.1 MPa over a wide range of temperatures, T = 210−460 K, and glycerol molar fractions, χ_g = 0.14, 4.95, 10, 15, 20, 25, 30, 40, and 50%. All simulations are performed for a system of N = 729 water molecules with N_g = 1, 38, 81, 129, 182, 243, 312, 486, and 729 glycerol molecules, depending on concentration. MD simulations of pure glycerol are performed for a system of N_g = 700 molecules. The molecules are placed in a cubic box with periodic boundary conditions. The box side length L varies with the system being studied but is found to be in the range of ∼25−55 Å.

Simulations are performed at constant pressure and temperature using the LAMMPS software package.[29] The temperature and pressure are controlled using a Nosé−Hoover-style thermostat and barostat employing the equations of motion described by Shinoda et al.[30] Following ref 27, the thermostat uses a time constant for temperature coupling of 0.1 ps, and the barostat uses a pressure relaxation time constant of 5 ps. Long-range electrostatic interactions are calculated using a particle−particle particle-mesh solver[31] with an accuracy of 10^{-4}. Lennard-Jones and Coulombic interactions are brought smoothly to zero from r_1 = 10 Å to r_2 = 11 Å using a polynomial switching function.

The starting configuration for a given concentration is prepared as follows. First, we perform an independent MD simulation of $N \approx$ 3000−5000 water molecules in a box at T = 300 K and P = 0.1 MPa and let the system equilibrate. Second, an independent MD simulation of a single glycerol molecule in a water bath is performed at T = 300 K using the SPC/E model[32] for water, from which 729 independent glycerol configurations (atom positions/velocities) are obtained. Third, the single-molecule glycerol configurations are used to locate N_g (≤729) molecules randomly in the previously equilibrated box of water. We ensure that no atom of a given molecule is within a distance of 3.5 Å from an atom of any other molecule in the system. Additional water molecules are removed randomly until a total of N = 729 water molecules remain in the system. The box is then compressed rapidly at 300 K until the experimental density of the corresponding solution at normal pressure is reached. The system is then simulated for an additional 1 ns. The resulting glycerol−water configuration is then used as the starting configuration for simulation runs at constant temperature T and pressure P = 0.1 MPa. Simulations are run for Δt_{sim} = 5−70 ns depending on the temperature, concentration, and mixture model. In all cases, we report results for only those temperatures at which the diffusion regime is reached by both water and glycerol (during the simulated times), i.e., the mean-square displacement (MSD) of water and glycerol obey $\mathrm{MSD}(t) \approx t$ for long times. At these temperatures, $\Delta t_{sim} > 2-3\ \tau$, where τ is the time at which glycerol's MSD equals 100 Å^2. This MSD corresponds roughly to the size of a glycerol molecule, ∼10 Å, and is larger than the typical separation between the central C atoms of nearest-neighbor glycerol molecules, ∼6 Å (ref 13). This allows us to study temperatures as low as T = 210 K for $\chi_g \leq$ 20% and 240 K for 20% < $\chi_g \leq$ 50%. In all cases, the simulation time step is 1.0 fs.

2.1. Force Fields. We consider three different glycerol−water mixture models obtained by combining two water models and two glycerol models. The glycerol models considered are (i) the model introduced by Reiling et al.[33] based on the CHARMM22 FF[34,35] (R-FF) and (ii) the model developed by Chelli et al.[11] and slightly modified by Blieck et al.,[12,13,36] based on the AMBER FF (BC-FF).[37] The interaction parameters that define these models are provided in the Supporting Information of ref 27. We note that in a previous work[27] we studied the properties of pure glycerol using BC-FF, R-FF, and three versions of the original OPLS-FF.[38] The simulations using the OPLS FFs indicate that liquid glycerol can form intramolecular HBs with an average O−O distance of ∼2.45 Å. This separation is much smaller than the typical O−O distance associated with a hydrogen bond (HB), which is ∼2.7−2.8 Å for the case of water. For this reason, in this work we consider only the BC and R-FF. Regarding the water models considered, we employ the original TIP3P water model developed by Jorgensen et al.[39] because both AMBER and CHARMM22 FFs were originally developed in conjunction with TIP3P water;[40−42] in addition, we perform simulations using the TIP4P/2005 water model developed by Abascal and Vega.[43,44] The TIP4P/2005 water model exhibits thermodynamic and dynamical properties that are closer to experimental values than to the properties of TIP3P water. The three mixture models studied are obtained by combining (i) the TIP3P water model with the R-FF of glycerol (briefly, R+TIP3P FF), (ii) the TIP3P water model with the BC-FF of glycerol (briefly, BC +TIP3P FF), and (iii) the TIP4P/2005 water model with the BC-FF of glycerol (briefly, BC+TIP4P/2005 FF). One of the goals of this work is to compare the performance of FFs (i), (ii), and (iii) with experimental data, this issue being a topic of practical relevance. A less evident goal of this work is to estimate the sensitivity of the properties of binary aqueous solutions to the FF considered. This is particularly important for the case of small flexible molecules, such as glycerol, that can change molecular conformations.

DOI: 10.1021/acs.jpcb.5b00439
J. Phys. Chem. B 2015, 119, 6250−6261

3. THERMODYNAMIC PROPERTIES

We study the following thermodynamic properties of glycerol−water mixtures, (A) density, (B) thermal expansion coefficient, (C) isothermal compressibility, and (D) isobaric specific heat, as a function of both temperature and concentration. We note that for a simple system, such as a single-phase mixture of water and glycerol with a constant number of moles, properties B−D constitute a basic set of thermodynamic response functions from which all others can be obtained.[45]

3.1. Density. The density of the glycerol−water mixtures as a function of temperature for the R+TIP3P and BC+TIP3P FFs is shown in Figure 1a. Our densities for the R+TIP3P mixture

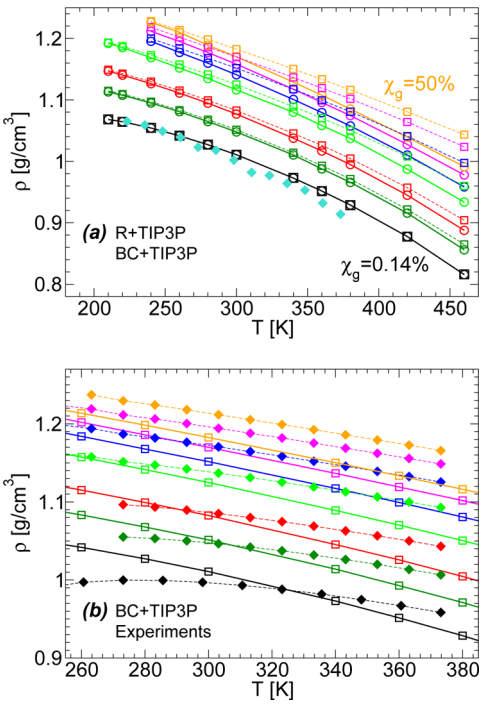

Figure 1. (a) Density as a function of temperature for water−glycerol mixtures at different glycerol molar fraction, χ_g. Empty circles and squares are results from MD simulations of TIP3P water with R-FF and BC-FF for glycerol, respectively; turquoise filled diamonds are densities of the original TIP3P water model from ref 60. (b) Comparison of density values obtained in experiments (filled diamonds) and MD simulations using the BC+TIP3P mixture model (squares, taken from (a)). Colors in (a) and (b) correspond to χ_g = 0.14% (black), 4.95% (dark green), 10% (red), 20% (green), 30% (blue), 40% (magenta), and 50% (orange). Experimental data for $\chi_g \geq$ 4.95% is taken from ref 51. Black diamonds in (b) are experimental data for pure water from ref 61. P = 0.1 MPa.

agree with the values reported in ref 46 for $\chi_g \leq$ 8.3% at T = 298 K and P = 0.1 MPa. In both cases, $\rho(T)$ decreases monotonically with increasing temperature. However, the densities predicted by the BC+TIP3P model are slightly larger than those obtained using the R+TIP3P model, particularly at high temperatures. Figure 1a also shows that at a given temperature the density difference between the two mixture models ($\Delta\rho$) increases with increasing concentration. For example, at T = 460 K, $\Delta\rho \approx$ 0.02 g/cm^3 at χ_g = 10% whereas $\Delta\rho \approx$ 0.06 g/cm^3 at χ_g = 50%. This value of $\Delta\rho$ is consistent with the difference in density between R-FF and BC-FF pure glycerol reported in ref 27. For example, these glycerol models predict pure glycerol densities that differ by $\Delta\rho \approx$ 0.08 g/cm^3 at T = 460 K.

The densities of the BC+TIP3P mixture model are compared to the corresponding experimental data in Figure 1b (similar conclusions apply for the R+TIP3P mixture model). At high temperatures, simulations underestimate the densities at all concentrations. The differences in density increase with increasing χ_g; for example, at T = 373 K, $\Delta\rho \approx$ 0.02 g/cm^3 at χ_g = 0.14% and $\Delta\rho \approx$ 0.04 g/cm^3 at χ_g = 50%. Instead, at low temperatures, simulations tend to overestimate the mixtures densities, with $\Delta\rho$ increasing upon cooling. This is shown explicitly in Figure 1b for $\chi_g \leq$ 20%, where the experimental and simulation $\rho(T)$ curves intersect. At $\chi_g >$ 20%, the experimental and simulation $\rho(T)$ curves are expected to intersect at $T <$ 260 K. It follows that the present model mixtures may be problematic with respect to studying the properties of glycerol−water solutions in the supercooled state.

Water is known to exhibit a density maximum at T = 277 K, implying that below this temperature there is a range of temperatures at which water expands upon isobaric cooling. It follows that at very low concentrations, glycerol−water mixtures should exhibit a density maximum as well. Indeed, the experimental data for $\chi_g \leq$ 10% in Figure 1b is consistent with the possibility that a density maximum exists at $T <$ 270 K. One may wonder if the R+TIP3P and BC+TIP3P mixture models may exhibit density maxima at low concentrations as well. Figure 1a shows that this is not the case, a result that may not be surprising given that the TIP3P water model does not exhibit a density maximum either (the density of TIP3P water decreases monotonically with increasing temperature; see Figure 1a). Unfortunately, as we will show in the next sections, many of the thermodynamic properties of the glycerol mixtures studied deviate from the corresponding experimental data due to the inability of TIP3P water to reproduce some of the properties of pure water.

A natural question is whether the results obtained with TIP3P water can be improved if a better water model is used. To address this issue, we calculate the density of the BC+TIP4P/2005 mixture model as a function of temperature and concentration (Figure 2a,b). We note that the TIP4P/2005 water model is perhaps one of the best rigid water models available, being able to reproduce many of water's anomalous properties, such as the density maximum at normal pressure.[43,44]

Figure 2a shows the densities of the BC+TIP3P and BC+TIP4P/2005 mixture models as a function of temperature for different χ_g values. Differences in density between the two models are noticeable, particularly at low temperatures and become smaller with increasing concentrations. (At high concentrations, the water model should have a minor effect on the thermodynamic properties of the mixtures because both models are based on the same glycerol FF.)

Interestingly, the water model drastically affects the qualitative behavior of $\rho(T)$. Specifically, the BC+TIP4P/2005 mixtures exhibit clear density maxima at ($T \approx$ 278 K, χ_g = 0.14%) and at ($T \approx$ 240 K, χ_g = 4.95%), as expected for the case of dilute aqueous solutions, whereas the BC+TIP3P mixture does not.

The densities predicted by the BC+TIP4P/2005 model are compared to the experimental densities in Figure 2b. A comparison of Figures 2b [BC+TIP4P/2005] and 1b [BC+TIP3P] indicates a remarkable improvement in the density

DOI: 10.1021/acs.jpcb.5b00439
J. Phys. Chem. B 2015, 119, 6250−6261

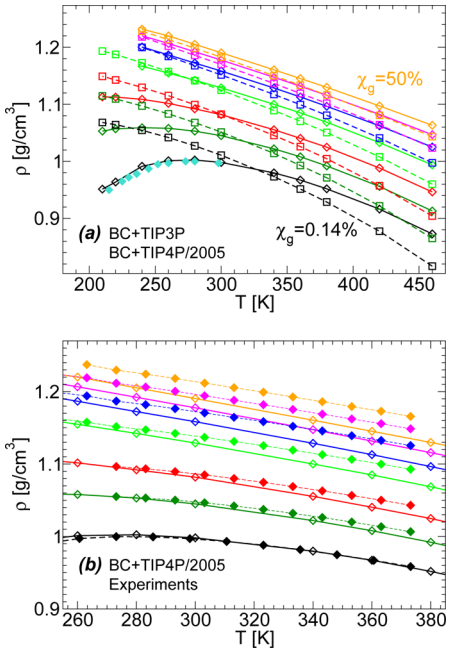

Figure 2. (a) Density as a function of temperature for water−glycerol mixtures at different glycerol molar fractions, χ_g. Empty diamonds and squares are the results for BC+TIP4P/2005 and BC+TIP3P mixture models, respectively. For comparison, the densities of TIP4P/2005 water from ref 43 are included (turquoise filled diamonds). (b) Comparison of density values obtained in experiments (filled diamonds) and MD simulations using the BC+TIP4P/2005 mixture model (empty diamonds, taken from (a)). Colors correspond to χ_g = 0.14% (black), 4.95% (dark green), 10% (red), 20% (green), 30% (blue), 40% (magenta), and 50% (orange).

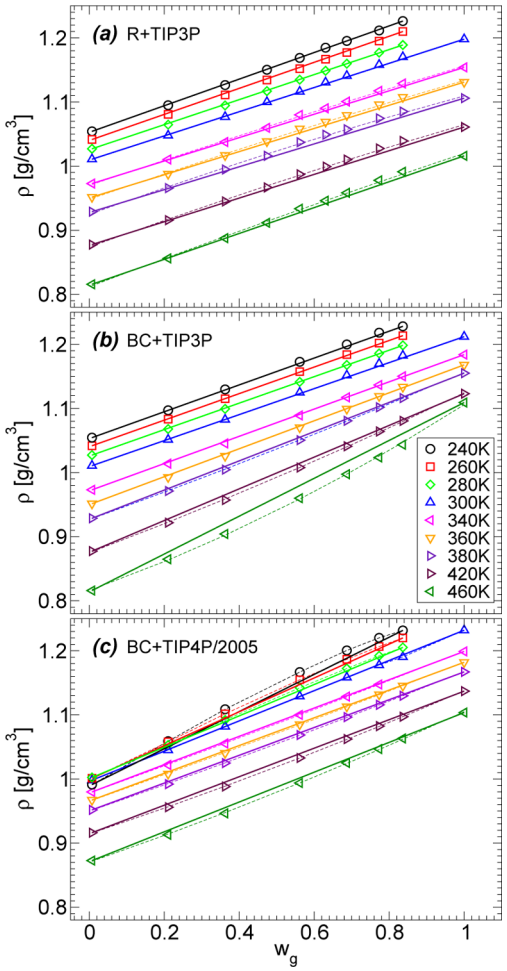

Figure 3. Density as a function of glycerol weight fraction for water−glycerol mixtures at different temperatures. (a) R+TIP3P, (b) BC +TIP3P, and (c) BC+TIP4P/2005 mixture model. The data is taken from Figures 1a and 2a for $w_g < 1$ and from ref 27 for $w_g = 1$. In (a) and (b), linear behavior in $\rho(w_g)$ is found at low temperatures, in agreement with experiments; in (c), linear behavior in $\rho(w_g)$ is found only at $T \approx 300$ K. Solid lines are fits using eq 1; dashed lines are fittings using quadratic polynomials. Error bars in density are smaller than the symbol size.

values of the mixtures when the TIP4P/2005 model is used, particularly at $\chi_g \leq 20\%$.

For practical applications, it may be useful to express the density of the glycerol−water mixtures as a function of glycerol weight fraction, w_g. Interestingly, experiments indicate that the densities of glycerol−water solutions and brine−glycerol mixtures across the whole glycerol concentration range[47,48] and for approximately $T < 350$ K are well described by the following expression

$$\rho(w_g, T) = (1 - w_g)\rho_w^0(T) + w_g\rho_g^0(T) \quad (1)$$

where $\rho_w^0(T)$ and $\rho_g^0(T)$ are the densities of pure water and glycerol at temperature T, respectively.

Figure 3a−c shows $\rho(w_g)$ for the R+TIP3P, BC+TIP3P, and BC+TIP4P/2005 mixture models, respectively, based on the data included in Figures 1a and 2a. The corresponding predictions of eq 1 are also included (solid lines). Interestingly, the three mixture models indicate that $\rho(w_g)$ increases approximately linearly with w_g, as observed in experiments. However, small deviations are observable. Specifically, the R +TIP3P (BC+TIP3P) mixture model slightly overestimates (underestimates) the density values predicted by eq 1 at high temperatures; the BC+TIP4P/2005 model underestimates the density values predicted by eq 1 at $T > 300$ K and overestimates the densities at $T < 300$ K.

3.2. Thermal Expansion Coefficient. The thermal expansion coefficient, $\alpha_P(T) = -\rho^{-1}(\partial\rho/\partial T)_P$, is another relevant thermodynamic property to benchmark the different water−glycerol models. The $\alpha_P(T)$ obtained from experiments and simulations is shown in Figure 4a−c for selected concentrations. In all cases, we obtain $\alpha_P(T)$ from Figures 1a,b and 2a by fitting $\rho(T)$ with a polynomial. (A fifth-order polynomial is used for the case of TIP4P/2005 and real water (inset of Figure 4c) as well as for BC+TIP4P/2005 mixtures with $\chi_g \leq 4.95\%$; a second-order polynomial is used in all other cases.)

Compared to experiment, all FFs overestimate $\alpha_P(T)$. For example, in the case of the R+TIP3P and BC+TIP3P mixture models (Figure 4a), $\alpha_P(T)$ at $T = 273$ K and $\chi_g = 10\%$ is approximately 2.3−2.4 times the corresponding experimental value. Figure 4a shows that in these cases, where the same TIP3P water model is employed, deviations in $\alpha_P(T)$ are slightly more pronounced in the case of the R-FF for all temperatures and concentrations. Replacing TIP3P water with TIP4P/2005 water considerably improves the results from simulations relative to experiments (Figure 2b). For example, the BC+TIP4P/2005 model predicts a value of $\alpha_P(T)$ at $T = 273$ K and $\chi_g = 10\%$ that is ∼1.3 times the corresponding experimental value. (See also the next paragraph.)

DOI: 10.1021/acs.jpcb.5b00439
J. Phys. Chem. B 2015, 119, 6250−6261

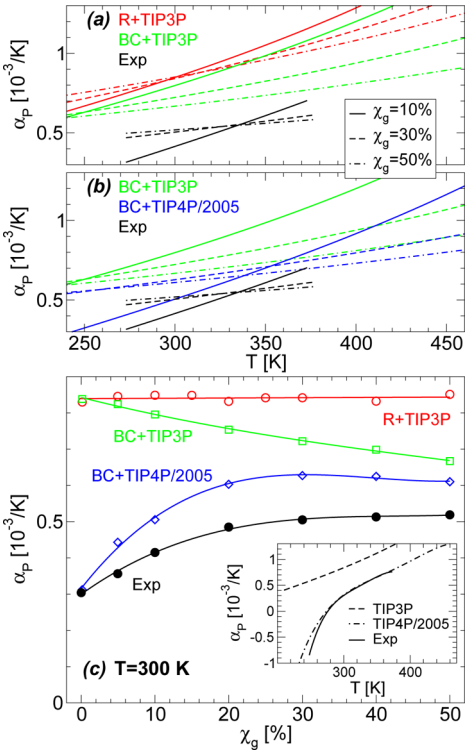

Figure 4. Thermal expansion coefficient of glycerol–water mixtures from MD simulations and experiments at P = 0.1 MPa. (a, b) α_P as a function of temperature for concentrations χ_g = 10, 30, and 50% (solid, dashed, and dotted–dashed lines, respectively). Black, red, green, and blue lines correspond, respectively, to experiments and MD simulations using the R+TIP3P, BC+TIP3P, and BC+TIP4P/2005 mixture models. Compared to experiments, all mixture models overestimate $\alpha_P(T)$. (c) α_P as a function of concentration at T = 300 K. Notable improvement is achieved when the TIP3P water model is replaced by the TIP4P/2005 water model. Inset: $\alpha_P(T)$ for TIP3P, TIP4P/2005, and real water. Relative errors are smaller than 10%.

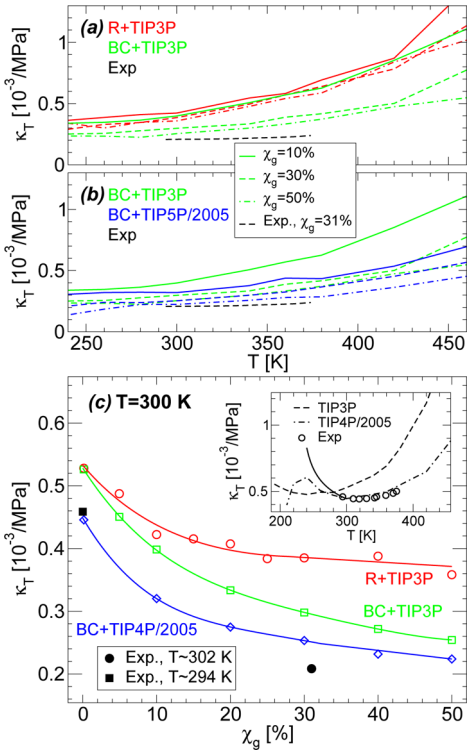

Figure 5. Isothermal compressibility κ_T of glycerol–water mixtures from MD simulations and experiments at P = 0.1 MPa. (a, b) κ_T as a function of temperature for concentrations χ_g = 10, 30, and 50% (solid, dashed, and dotted–dashed lines, respectively). Black, red, green, and blue lines correspond, respectively, to experiments and MD simulations using the R+TIP3P, BC+TIP3P, and BC+TIP4P/2005 mixture models. All models show qualitatively the same behavior of $\kappa_T(T)$. Comparison between simulations at χ_g = 30% and experiments from ref 62 at χ_g = 31% shows that all models overestimate $\kappa_T(T)$ and that deviations in $\kappa_T(T)$ are less pronounced for the BC+TIP4P/2005 mixture model. (c) κ_T as a function of concentration at T = 300 K. On the basis of the limited experimental data [black square (T = 302 K) and circle (T = 294 K), from ref 62], the BC+TIP4P/2005 mixture model apparently reproduces the experimental data very closely. Inset: Comparison of water isothermal compressibility from simulations using the TIP3P and TIP4P/2005 models as well as from experiments. Experimental data (circles) is from ref 62; the solid line is the power-law fit to the experimental data given in ref 63. Relative errors are smaller than 10%.

The effects of concentration on α_P are shown in Figure 4c for T = 300 K. Clearly, the α_P predicted by the BC+TIP4P/2005 mixture model is closest to the experimental α_P among the FFs studied. In particular, only the BC+TIP4P/2005 mixture model is able to reproduce the decrease in α_P as $\chi_g \to 0$. Evidently, it is the TIP4P/2005 model that leads to better performance. Indeed, the inset of Figure 4c shows that TIP4P/2005 water predicts the correct α_P of water over a wide range of temperatures whereas the TIP3P model does not. We note that the influence of the water model in the mixture models' $\alpha_P(T)$ is not limited to the case $\chi_g \to 0$ but is relevant up to concentrations of at least χ_g = 50%.

3.3. Isothermal Compressibility. The isothermal compressibility of the glycerol–water mixtures, $\kappa_T = \rho^{-1}(\partial\rho/\partial P)_T$, is obtained from the volume fluctuations of the system, δV, using the relationship[49]

$$\kappa_T = \frac{\langle \delta V^2 \rangle}{k_B T \langle V \rangle} \tag{2}$$

where k_B is the Boltzmann constant and the brackets indicate the average over system configurations. κ_T is shown in Figure 5a,b for χ_g = 10, 30, and 50% and P = 0.1 MPa. For comparison, results from experiments at χ_g = 31% are included. Qualitatively, all models predict an increase in $\kappa_T(T)$ with increasing temperature, although the data at χ_g = 30–31% suggests that the increase in $\kappa_T(T)$ is milder in experiment than in simulations. Accordingly, all mixture models overestimate κ_T at high temperatures. For example, in the case of the R+TIP3P model at χ_g = 30% and T = 373 K, simulations predict a value for κ_T that is more than twice the corresponding experimental value (Figure 5a).

As for the case of $\alpha_P(T)$, the experimental κ_T is best reproduced by the BC+TIP4P/2005 mixture model. This is evident in Figure 5c, which shows κ_T as a function of glycerol concentration at T = 300 K. Although the available experimental data in Figure 5c is limited, only for χ_g = 0 and 31%, the BC+TIP4P/2005 mixture model performs much better than the other two models based on TIP3P water. Hence, by analogy to the cases of α_P and ρ, replacing TIP3P water with TIP4P/2005 water improves the values of $\kappa_T(\chi_g)$ relative to experiment. Indeed, as shown in the inset of Figure 5c, the TIP4P/2005 water model remarkably reproduces the

DOI: 10.1021/acs.jpcb.5b00439
J. Phys. Chem. B 2015, 119, 6250–6261

experimental compressibility of water in the range of $T \approx 295-373$ K; the TIP3P model does not.

3.4. Isobaric Specific Heat. The next thermodynamic property that we will discuss is the isobaric specific heat, $c_P(T) = (\partial H/\partial T)_P$. We obtain $c_P(T)$ by calculating the enthalpy of the system as a function of temperature, $H(T)$. In all cases, $H(T)$ is practically a linear function of T for $\chi_g \geq 4.95\%$. Hence, at these concentrations, we fit $H(T)$ with a second-order polynomial and obtain $c_P(T)$ by differentiating $H(T)$ with respect to T. Our choice of using a second-order polynomial to fit $H(T)$ is also motivated by experiments in glycerol[50] and water−glycerol mixtures at $\chi_g \geq 25\%$ and $T < 275$ K[51] that show that $c_P(T) \propto T$. However, we note that at low concentrations (e.g., $\chi_g < 4.95\%$) $c_P(T)$ may exhibit a nonlinear T dependence because for the case of water at low temperatures, $c_P(T)$ indeed decreases nonlinearly with increasing temperature[52] (inset of Figure 6c). Accordingly, in the case of TIP3P and TIP4P/2005

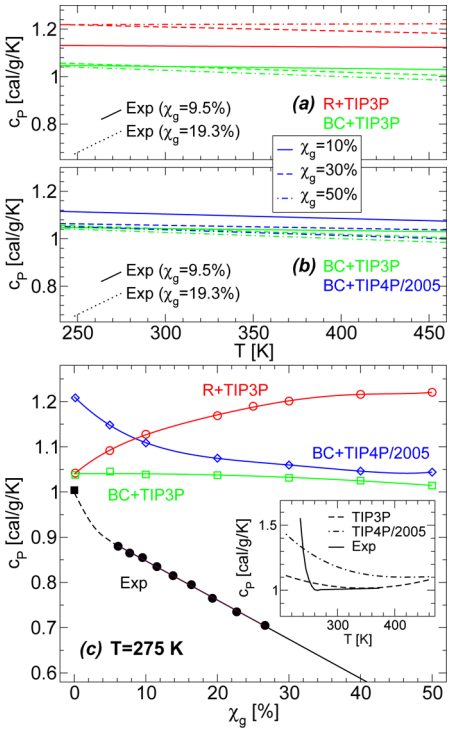

Figure 6. Isobaric specific heat of glycerol−water mixtures from MD simulations and experiments at $P = 0.1$ MPa. (a, b) c_P as a function of temperature for concentrations $\chi_g = 10$, 30, and 50% (solid, dashed, and dotted−dashed lines, respectively). Black, red, green, and blue lines correspond, respectively, to experiments and MD simulations using the R+TIP3P, BC+TIP3P, and BC+TIP4P/2005 mixture models. None of the mixture models considered are able to reproduce the T dependence of $c_P(T)$. (c) c_P as a function of concentration at $T = 275$ K. The mixture models are not able to reproduce the qualitative behavior of $c_P(\chi_g)$ independently of the water model used. Inset: c_P as a function of temperature for TIP3P and TIP4P/2005 water and experiments. Experimental data is from refs 51 (water−glycerol mixtures) and 52 (water). Relative errors are smaller than 2%.

(pure) water (inset of Figure 6c) and for mixtures with concentrations with $\chi_g = 0.14\%$, we use a fourth-order polynomial to obtain $c_P(T)$. (Similar results are obtained by fitting polynomials of order 3−5).

Figure 6a,b shows $c_P(T)$ for the three mixture models studied, together with experimental values from ref 51 at selected concentrations. None of the mixture models considered are able to reproduce the T dependence of $c_P(T)$. Moreover, the models studied predict $c_P(T)$ with very different T dependences. However, this is not unexpected because the $c_P(T)$ of TIP3P and TIP4P/2005 water exhibits a qualitatively different dependence on T (inset of Figure 6c). A comparison of $c_P(T)$ between simulations and experiments (Figure 6a,b) shows that the three mixture models studied overestimate the experimental specific heat. For example, at $\chi_g = 9.5-10\%$ and $T = 263$ K, the model mixtures predict a c_P that is ∼1.3−2.2 times the corresponding experimental value. We note that the specific heats of R-FF and BC-FF (pure) glycerol are larger than the experimental values by a factor of 1.3−2.4, and a similar situation holds for both TIP3P and TIP4P/2005 water (inset of Figure 6c). Classical MD simulations in general tend to provide larger $c_P(T)$ values than expected, and better agreement between simulation and experiment can be achieved after quantum corrections are included (e.g., ref 14).

Regardless of the limitations of MD simulations in reproducing the experimental isobaric specific heats, it is important for thermodynamic and computational studies to compare the dependence of specific heat on concentration. To do this, we show in Figure 6c the specific heat as a function of χ_g at $T = 275$ K. None of the mixture models is able to capture the qualitative χ_g dependence of the specific heat. Interestingly, the experimental $c_P(\chi_g)$ increases as $\chi_g \to 0$, and such behavior is captured only by the BC+TIP4P/2005 mixture model.

4. DYNAMICAL PROPERTIES

In this section, we study the diffusion coefficients of water and glycerol, D_w and D_g, as functions of temperature and glycerol concentration. The diffusion coefficient of water is obtained from the mean-square displacement of the oxygen atoms using Einstein's relationship $\langle r^2(t)\rangle = 6Dt$ where t is the time, which is valid in the diffusive regime. Similarly, the diffusion coefficient of glycerol is obtained using Einstein's relationship where $\langle r^2(t)\rangle$ is the mean-square displacement of glycerol's central carbon atom.

4.1. Temperature Dependence of the Glycerol Diffusion Coefficient. Figure 7a shows $D_g(T)$ from MD simulations using the R+TIP3P and BC+TIP3P models. The values of $D_g(T)$ for the case of BC+TIP4P/2005 and BC +TIP3P are shown in Figure 7b. In all cases, the T dependence of the glycerol diffusion coefficient is well-approximated by the Vogel−Tamman−Fulcher (VTF) equation[53]

$$D(T) = A_0\sqrt{T}\,\exp\left(-\frac{B}{T - T_0}\right) \tag{3}$$

where A_0, B, and T_0 are fitting parameters. The VTF equation is commonly used to model the T dependence of the diffusion coefficient of liquids at low temperatures.[54−56] As shown in ref 57, the experimental diffusion coefficient of pure glycerol is well-fitted by eq 3, and for concentrations of $85\% \leq \chi_g < 100\%$, the experimental $D_g(T)$ obeys a VTF equation but with apparent deviations at low temperatures. In the case of computer simulations of pure glycerol, we found that $D_g(T)$ obeys eq 3 as well.[27]

Figure 7a shows the effect of changing the glycerol FF on $D_g(T)$ for the case of TIP3P water. We note that these effects may be general and valid for other binary aqueous solutions. At very low concentrations, e.g., $\chi_g = 0.14\%$, $D_g(T)$ is practically independent of the glycerol FF employed. This suggests that

DOI: 10.1021/acs.jpcb.5b00439
J. Phys. Chem. B 2015, 119, 6250−6261

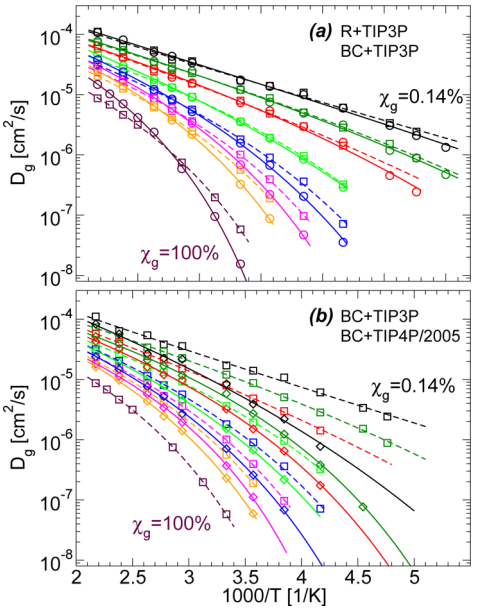

Figure 7. Diffusion coefficient of glycerol in glycerol−water mixtures from computer simulations using (a) R+TIP3P (circles) and BC+TIP3P FFs (squares) and (b) BC+TIP3P (squares) and BC+TIP4P/2005 FFs (diamonds).[64] Data correspond to concentrations of χ_g = 0.14% (black), 4.95% (dark green), 10% (red), 20% (green), 30% (blue), 40% (magenta), 50% (orange), and 100% (maroon). Lines are fittings using the VTF equation (eq 3).

the diffusivity of glycerol at very low concentrations is mainly determined by the water model used and not by the specific water−glycerol interactions. However, as χ_g increases, differences in the models' $D_g(T)$ at a given temperature become greater. It follows that the maximum difference between the models' $D_g(T)$ occurs at χ_g = 100%.

The case where the water model is replaced, leaving the glycerol FF (BC-FF) unchanged, is shown in Figure 7b. In this case, $D_g(T)$ becomes less sensitive to the mixture model as the concentration increases, which is expected because for $\chi_g \rightarrow$ 100% both mixture models reduce to pure BC-FF glycerol. As $\chi_g \rightarrow$ 0%, the water model plays a central role and differences in the mixture models' $D_g(T)$ become relevant. This is particular evident in the data of Figure 7b for χ_g = 4.95%; at low temperatures, the difference in the models' $D_g(T)$ can differ by approximately 1 order of magnitude. This is larger than the differences in $D_g(T)$ observed in Figure 7a (where the BC-FF is replaced by the R-FF, while the same TIP3P water model is used), where $D_g(T)$ may vary by a factor of <4. Interestingly, in all cases, the differences in $D_g(T)$ among the three mixture models become more pronounced at low temperatures, when molecular details become relevant.

The diffusivities of glycerol in the different mixture models can be compared semiquantitatively by looking at the corresponding VTF fitting parameters. We stress that these parameters should be taken with caution and are only indicative of the T dependence of $D_g(T)$; fitting slightly different sets of data points or altering the fitting procedure can produce significant variations in the fitting parameters (e.g., ref 27). The VTF parameters for glycerol diffusion coefficients, for all concentrations and model mixtures studied, are shown in Figure 8. Parameter A_0 increases monotonically with decreasing glycerol concentration in all model systems. Parameters B and T_0 for water−glycerol mixtures have been measured in the

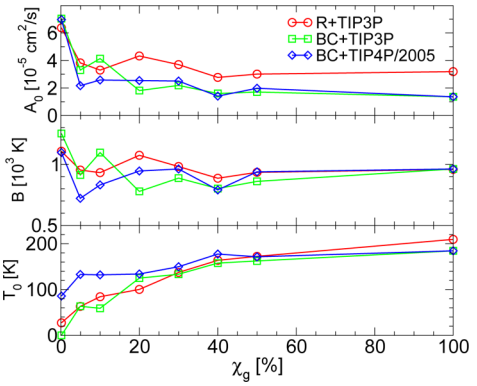

Figure 8. Fitting parameters of the VTF equation (eq 3) for the diffusion coefficient of glycerol at different concentrations. Circles, squares, and diamonds represent parameters for R+TIP3P, BC+TIP3P, and BC+TIP4P/2005 models.

range χ_g = 85−100%, and it has been shown that they both decrease with decreasing χ_g.[57] In particular, parameter B reported from experiments in ref 57 for χ_g = 85−100% is in the range of 1200−1400 K. These values are slightly larger than the corresponding values from the mixture models studied, $B \approx$ 800−1000 K. Parameter T_0 is particularly interesting because it is close to the glass-transition temperature of the mixture. For example, for pure glycerol, experiments show that T_0 = 170 K and T_g = 190 K. Our simulations predict that for χ_g = 100%, T_0 = 180−210 K for all models studied, which is slightly larger than the experimental value. We note that as $\chi_g \rightarrow$ 0, one would expect that T_0 decreases toward a value slightly smaller than the water glass-transition temperature, ∼136 K. This seems to be the case for only the BC+TIP4P mixture model. In the case of R+TIP3P and BC+TIP3P, $T_0 \rightarrow$ 0 as $\chi_g \rightarrow$ 0, implying that the VTF equation becomes an Arrhenius equation or that non-Arrhenius behavior develops at even lower temperatures than those studied.

It is natural to ask which FF performs better in terms of glycerol dynamics when compared to experiments. To address this question, we include in Figure 9 the values of $D_g(T)$ obtained from computer simulation as well as the corresponding values estimated from experiments at selected concentrations; additional comparisons between experimental and MD simulation diffusivities are provided in section 4.4. The experimental values of $D_g(T)$ are estimated from viscosity measurements, η, combined with the Stokes−Einstein (SE) relationship

$$D_g = \frac{k_B T}{6\pi\eta r_H} \quad (4)$$

where k_B is the Boltzmann constant and r_H is the hydrodynamic radius of glycerol. The viscosity data is obtained from ref 51. Three different hydrodynamic radii are considered, r_H = 1.4, 2.0, and 2.5 Å, which cover the range of values determined experimentally in ref 57 for χ_g = 80−95%. Our procedure to estimate D_g is supported by the experiments in ref 57, where it is shown that the SE relation holds for water−glycerol mixtures at approximately T > 295 K (or 1000/T < 3.4) and for χ_g = 80−95%. Moreover, these results suggest that the temperature range where the SE relationship holds increases as χ_g decreases.

Figure 9a−d shows that BC+TIP4P/2005 FF practically reproduces the experimental values of $D_g(T)$ at all concentrations and performs better than the BC+TIP3P and R+TIP3P

DOI: 10.1021/acs.jpcb.5b00439
J. Phys. Chem. B 2015, 119, 6250−6261

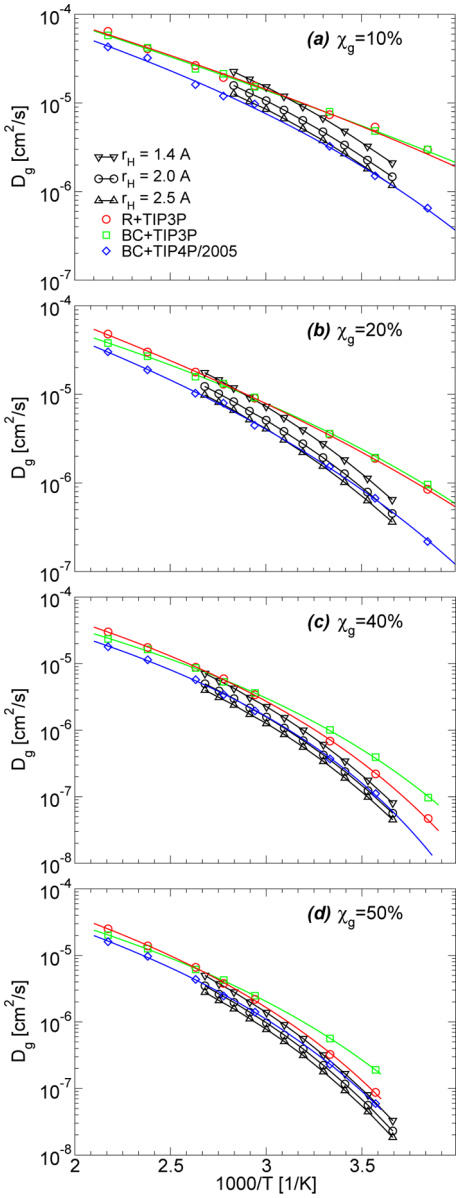

Figure 9. Glycerol diffusion coefficient in glycerol−water mixtures from experiments (black symbols) and computer simulations using R+TIP3P (red circles), BC+TIP3P (green squares), and BC+TIP4P/2005 FF (blue diamonds). Experimental diffusion coefficients are obtained from viscosity data using the Stokes−Einstein relationship with different hydrodynamic radii r_H. (See the text.)

mixtures. This is evident at low temperatures and, in particular, at low concentrations where the differences between TIP4P/2005 and TIP3P water are important. For example, under normal conditions, the diffusion coefficient of TIP4P/2005 water is ~2.1 × 10^{-9} m^2/s,[43] close to the corresponding experimental value, 2.3 × 10^{-9} m^2/s;[58] the diffusion coefficient of TIP3P water is 5.1 × 10^{-9} m^2/s.[40]

4.2. Temperature Dependence of the Water Diffusion Coefficient. Next, we discuss briefly water dynamics in the glycerol−water mixtures studied. The diffusion coefficient of water, $D_w(T)$, is shown in Figure 10a for the R+TIP3P and BC+TIP3P models; the results using the BC+TIP4P/2005 and BC+TIP3P models are shown in Figure 10b. As for the case of glycerol, all mixture models indicate that $D_w(T)$ can be well approximated by a VTF equation at all concentrations studied.

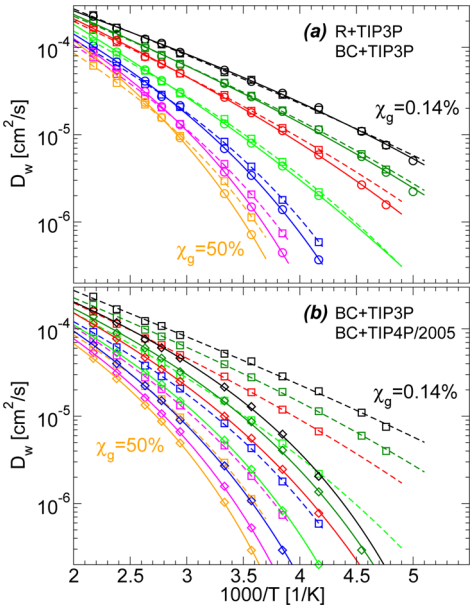

Figure 10. Diffusion coefficient of water in glycerol−water mixtures from computer simulations using R+TIP3P (circles), BC+TIP3P (squares), and BC+TIP4P/2005 FF (diamonds).[64] Data corresponds to concentrations of χ_g = 0.14, 4.95, 10, 20, 30, 40, and 50% (top to bottom). Lines are fittings using the VTF equation (eq 3).

Figure 10a shows that the differences in $D_w(T)$ for TIP3P water are relatively small, differing by up to a factor of 2, when the glycerol model is changed from BC-FF to R-FF. Instead, Figure 10b indicates that differences in $D_w(T)$ are relatively large when the water model is substituted and the glycerol FF is unchanged. Specifically, at low temperatures, differences in $D_w(T)$ between the mixture models can be larger than 1 order of magnitude. Figure 10a,b indicates that the water model can play a more relevant role than the glycerol FF in determining $D_w(T)$ in the water−glycerol mixtures, even at concentrations of as high as χ_g = 50% (glycerol weight fraction w_g = 84%).

The VTF parameters used to fit $D_w(T)$ are included in Figure 11. The data of Figure 11 is rather noisy, and it is difficult to specify a trend, particularly for $A_0(\chi_g)$ and $B(\chi_g)$. In the case of T_0 for water, we note that T_0 decreases as the amount of glycerol is reduced.

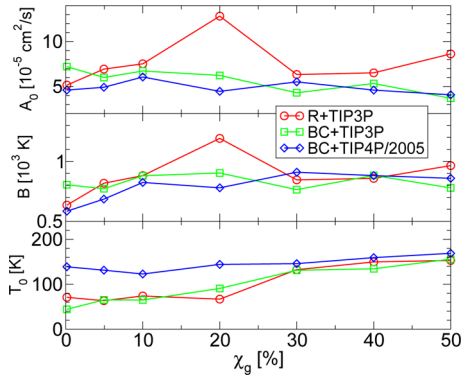

Figure 11. Fitting parameters of the VTF equation (eq 3) for the diffusion coefficient of water in glycerol−water mixtures at different concentrations. Circles, squares, and diamonds represent parameters for R+TIP3P, BC+TIP3P, and BC+TIP4P/2005 models.

DOI: 10.1021/acs.jpcb.5b00439
J. Phys. Chem. B 2015, 119, 6250−6261

4.3. Decoupling of Glycerol and Water Diffusion Coefficients upon Cooling. A comparison of Figures 7 and 10 shows that for a given concentration, $D_g(T) < D_w(T)$ for all temperatures studied. To explore what the relative effect of cooling is on water and glycerol translational motion, we include in Figure 12a–c $D_w(T)/D_g(T)$ for all mixture models

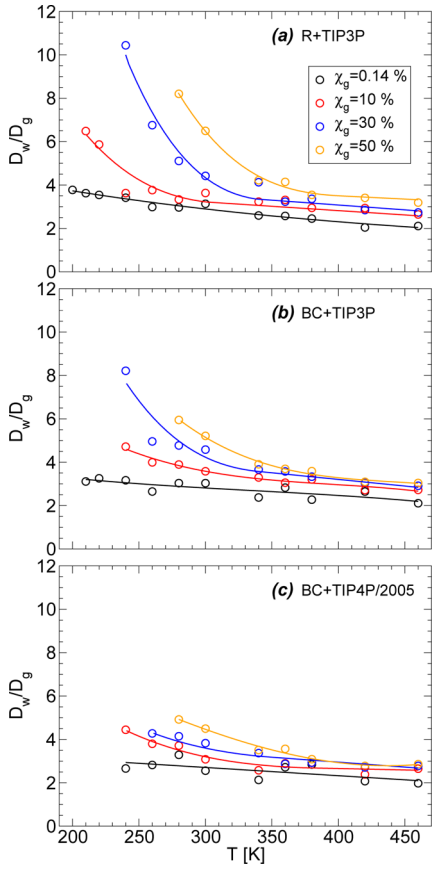

Figure 12. Ratio of water diffusion coefficient to glycerol diffusion coefficient as a function of temperature for (a) R+TIP3P, (b) BC+TIP3P, and (c) BC+TIP4P/2005 FFs. Decoupling of $D_g(T)$ and $D_w(T)$ occurs upon cooling in all mixture models. This is particularly evident in the TIP3P water-based mixtures where lower temperatures are accessible.

studied; the data is obtained from Figures 7 and 10. All mixture models indicate that $D_w(T)/D_g(T) \approx 2.5–3.5$ at $T = 460$ K for $\chi_g > 0.14\%$; we exclude the $\chi_g = 0.14\%$ case because the data is particularly noisy at this low concentration. This implies that, at high temperature, the water mean-square displacement (MSD) is roughly 3 times the MSD of glycerol. Interestingly, upon cooling, $D_w(T)/D_g(T)$ increases monotonically in all mixture models. In Figure 12a–c, this phenomenon is more pronounced for the R+TIP3P mixture than in the cases of BC+TIP3P and BC+TIP4P/2005 mixtures. For the R+TIP3P mixture, glycerol slows down relative to water by a factor of up to 10 (Figure 12a). Such a decoupling of water and glycerol translational motion becomes more evident at high concentrations. Our results suggest an interesting picture for high concentration glycerol–water solutions in which cooling may vitrify the glycerol matrix at temperatures above the temperature at which water is trapped in the glass state. In particular, this picture implies that there should be a range of temperatures at which water may diffuse in an immobile matrix of glycerol molecules.

4.4. Concentration Effects on Water and Glycerol Diffusivity. From a practical point of view, it is important to compare the effects of concentration on water and glycerol diffusivities. Accordingly, we show in Figure 13 both water and

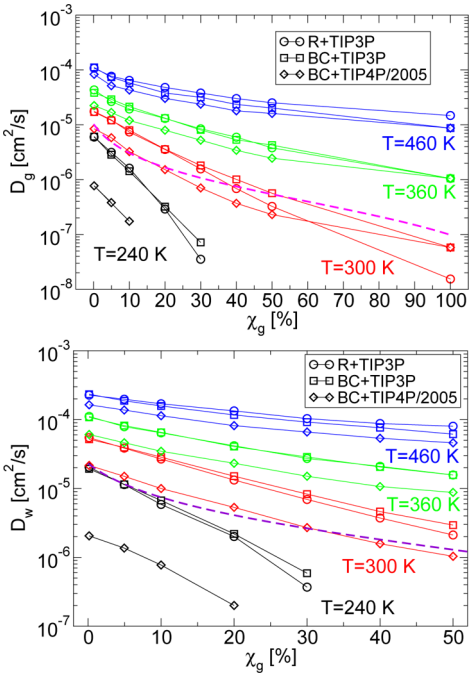

Figure 13. Diffusion coefficient of (top) glycerol and (bottom) water in glycerol–water mixtures as a function of concentration from computer simulations using R+TIP3P (circles), BC+TIP3P (squares), and BC+TIP4P/2005 FFs (diamonds). Magenta dashed lines in (a) and (b) are the analytical expressions given in ref 59 for the case $T = 298$ K based on experimental data. The diffusivities predicted by the BC+TIP4P/2005 mixture model are remarkably close to the corresponding experimental data.

glycerol diffusion coefficients as a function of χ_g; the data is obtained from Figures 7 and 10. All mixture models indicate that glycerol and water dynamics slow down monotonically with increasing amounts of glycerol for $\chi_g = 0–50\%$. This trend must continue until all of the water is removed, $\chi_g = 100\%$, as one can conclude from Figure 7a,b. We note that all mixtures predict the same qualitative behavior of $D_g(\chi_g)$ and $D_w(\chi_g)$.

Experimental data for D_g and D_w as a function of concentration is reported in ref 59 for $T = 298$ K. This data is included in Figure 13a,b. Again, it is found that the values of D_g and D_w predicted by the BC+TIP4P/2005 mixture model are closer to the corresponding experimental diffusivities than in the cases of BC+TIP3P and R+TIP3P models. This is evident for the case of water at all concentrations studied ($\chi_g = 0–50\%$, Figure 13b) and for glycerol at low concentrations (Figure 13a).

5. SUMMARY AND DISCUSSION

In this work, we studied the ability of computer simulations to reproduce thermodynamic (ρ, α_P, κ_T, and c_P) and dynamical (D_g and D_w) properties of glycerol–water mixtures at $P = 0.1$ MPa, covering a wide range of temperatures ($T = 210–460$ K) and glycerol concentrations ($\chi_g = 0–100\%$). One of the main goals of this work was to test the sensitivity of computer

DOI: 10.1021/acs.jpcb.5b00439
J. Phys. Chem. B 2015, 119, 6250–6261

simulation results to the mixture model employed. This is particularly important for flexible molecules, such as glycerol, that can adopt multiple molecular conformations. Our conclusions are based on three different mixture models: R+TIP3P, BC+TIP3P, and BC+TIP4P/2005.

The first property studied was the density. It was found that the three models underestimate the density of the mixtures at high temperatures. At low temperatures, the models tend to overestimate the experimental densities, with deviations increasing upon cooling and for decreasing χ_g. This may be problematic in computational studies focusing on the supercooled liquid states of water−glycerol solutions.

The three mixture models were compared to experiment in terms of basic thermodynamic response functions α_P, κ_T, and c_P. It was found that all of the models overestimate these properties. In the case of α_P and κ_T, MD simulations predict deviations that depend on temperature, concentration, and the mixture model considered. At T = 273 K and χ_g = 10%, the values of α_P from computer simulations and experiments differ by a factor of ∼1.3−2.4 (Figure 4a,b). Differences in κ_T between the mixture models and experiments are of the same order of magnitude; e.g., at T = 273 K and χ_g = 30%, the experimental and computer simulation values of κ_T differ by a factor of ∼1.5−2 (Figure 5a,b). Nonetheless, all mixture models studied were able to reproduce the temperature dependence of $\alpha_P(T)$ and $\kappa_T(T)$ qualitatively, both increasing with increasing T. Regarding the specific heat of the mixtures, results from MD simulations are at odds with experiment. However, this is not surprising because it is well known that classical MD simulations overestimate the specific heat of liquids. In this case, quantum corrections are needed.[14]

The dynamics of the mixture models were characterized in terms of glycerol and water (translational) diffusion coefficients. For all concentrations and FFs studied, it was found that both D_g and D_w can be well approximated by the VTF equation. A comparison of glycerol's diffusivity with available experimental data indicates that the mixture models provide good estimations of D_g, in particular, in the case of the TIP4P/2005 model. An interesting observation follows when comparing glycerol and water diffusion coefficients. All mixture models indicate a decoupling between glycerol and water diffusivities, with D_w/D_g increasing as T decreases. In the case of the TIP3P water-based mixture models the decoupling between water and glycerol dynamics is strong; for example, at χ_g = 50%, D_w/D_g increases from roughly 3−3.5 at T = 460 K to 6−8 at T = 280 K. In the case of the BC+TIP4P/2005 model, D_w/D_g increases from roughly 3 at T = 460 K to ∼5 at T = 280 K. This suggests that for water−glycerol mixtures, glycerol tends to vitrify at higher temperatures than water, and hence it may be possible to find a range of temperatures where water remains (weakly) mobile in a vitrified glycerol matrix.

We conclude by stressing the importance of the water model in determining the properties of the water−glycerol mixtures. This is particularly relevant if one is interested in the performance of the aqueous solution over a wide range of thermodynamic conditions. Computer simulations indicate that the water model employed affects the properties of the mixtures at high concentrations, as high as χ = 50% (glycerol weight fraction w_g = 0.84). This explains why the BC+TIP4P/2005 model performs much better than the R+TIP3P and BC+TIP3P models. After all, the TIP4P/2005 water model is remarkably successful in reproducing the thermodynamic and dynamical properties of real water. The BC+TIP4P/2005 mixture model considerably outperforms the BC+TIP3P and R+TIP3P models in reproducing experimental thermodynamic properties ρ, α_P, κ_T, and c_P as well as diffusion coefficients D_g and D_w. This conclusion holds at P = 0.1 MPa and for a wide range of temperature (T = 210−460 K) and glycerol concentrations (χ_g = 0−50%). In addition, only the BC+TIP4P/2005 mixture model was able to exhibit a density maximum at low concentrations, as must be the case in very dilute aqueous solutions.

The present work is part of a series of computational studies that we are performing on water−glycerol mixtures. In the present work, the focus is on thermodynamic and dynamical properties of the target mixtures; the structural properties of the mixtures (e.g., glycerol conformations, radial distribution functions, hydrogen-bond statistics, etc.) will be presented in a separate work. We hope that these studies will provide background information (thermodynamic, dynamics, structure) on glycerol−water mixtures that may be useful for the study of more complex systems.

AUTHOR INFORMATION

Corresponding Author

*E-mail: ngiovambattista@brooklyn.cuny.edu.

Notes

The authors declare no competing financial interest.

ACKNOWLEDGMENTS

We thank S. V. Buldyrev for fruitful discussions and M. Tomkiewicz for bringing ref 59 to our attention. Support for this project was provided by a PSC-CUNY Award, jointly funded by The Professional Staff Congress and The City University of New York. This research was supported, in part, under National Science Foundation grants CNS-0958379 and CNS-0855217 and the City University of New York High Performance Computing Center at the College of Staten Island.

REFERENCES

(1) Scheele, K. W. Findings Concerning a Particular Sweet Substance in Expressed Oils and Fatty Substances. *K. Sven. Vetenskapsakad. Hand.* **1783**, *4*, 324−329.

(2) Lawrie, J. W. *Glycerol and the Glycols*; The Chemical Catalog Company, Inc.: New York, 1928.

(3) *Nothing Takes the Place of Glycerine: 1583 Ways to Use it*; Soap and Detergent Association: New York, 1949.

(4) Polge, C.; Smith, A. U.; Parkes, A. S. Revival of Spermatozoa after Vitrification and Dehydration at Low Temperatures. *Nature* **1949**, *164*, 666−666.

(5) Pagliaro, M.; Rossi, M. *The Future of Glycerol*; The Royal Society of Chemistry: UK, 2010.

(6) Gu, Y.; Jérôme, F. Glycerol as a Sustainable Solvent for Green Chemistry. *Green Chem.* **2010**, *12*, 1127−1138.

(7) Root, L. J.; Stillinger, F. H. Short-Range Order in Glycerol. A Molecular Dynamics Study. *J. Chem. Phys.* **1989**, *90*, 1200−1208.

(8) Root, L. J.; Berne, B. J. Effect of Pressure on Hydrogen Bonding in Glycerol: A Molecular Dynamics Investigation. *J. Chem. Phys.* **1997**, *107*, 4350−4357.

(9) Dashnau, J. L.; Nucci, N. V.; Sharp, K. A.; Vanderkooi, J. M. Hydrogen Bonding and the Cryoprotective Properties of Glycerol/Water Mixtures. *J. Phys. Chem. B* **2006**, *110*, 13670−13677.

(10) Callam, C. S.; Singer, S. J.; Lowary, T. L.; Hadad, C. M. Computational Analysis of the Potential Energy Surfaces of Glycerol in the Gas and Aqueous Phases: Effects of Level of Theory, Basis Set, and Solvation on Strongly Intramolecularly Hydrogen-bonded Systems. *J. Am. Chem. Soc.* **2001**, *123*, 11743−11754.

DOI: 10.1021/acs.jpcb.5b00439
J. Phys. Chem. B 2015, 119, 6250−6261

(11) Chelli, R.; Procacci, P.; Cardini, G.; Valle, R. G. D.; Califano, S. Glycerol Condensed Phases Part I. A Molecular Dynamics Study. *Phys. Chem. Chem. Phys.* **1999**, *1*, 871−877.
(12) Blieck, J.; Affouard, F.; Bordat, P.; Lerbret, A.; Descamps, M. Molecular Dynamics Simulations of Glycerol Glass-forming Liquid. *Chem. Phys.* **2005**, *317*, 253−257.
(13) Egorov, A. V.; Lyubartsev, A. P.; Laaksonen, A. Molecular Dynamics Simulation Study of Glycerol-Water Liquid Mixtures. *J. Phys. Chem. B* **2011**, *115*, 14572−14581.
(14) Caleman, C.; van Maaren, P. J.; Hong, M.; Hub, J. S.; Costa, L. T.; van der Spoel, D. Force Field Benchmark of Organic Liquids: Density, Enthalpy of Vaporization, Heat Capacities, Surface Tension, Isothermal Compressibility, Volumetric Expansion Coefficient, and Dielectric Constant. *J. Chem. Theory Comput.* **2012**, *8*, 61−74.
(15) Chen, C.; Li, W. Z.; Song, Y. C.; Yang, J. Hydrogen Bonding Analysis of Glycerol Aqueous Solutions: A Molecular Dynamics Simulation Study. *J. Mol. Liq.* **2009**, *146*, 23−28.
(16) Kyrychenko, A.; Dyubko, T. S. Molecular Dynamics Simulations of Microstructure and Mixing Dynamics of Cryoprotective Solvents in Water and in the Presence of a Lipid Membrane. *Biophys. Chem.* **2008**, *136*, 23−31.
(17) Averett, D.; Cicerone, M. T.; Douglas, J. F.; de Pablo, J. J. Fast Relaxation and Elasticity-related Properties of Trehalose-glycerol Mixtures. *Soft Matter* **2012**, *8*, 4936−4945.
(18) Yongye, A. B.; Foley, B. L.; Woods, R. J. On Achieving Experimental Accuracy from Molecular Dynamics Simulations of Flexible Molecules: Aqueous Glycerol. *J. Phys. Chem. A* **2008**, *112*, 2634−2639.
(19) Politi, R.; Sapir, L.; Harries, D. The Impact of Polyols on Water Structure in Solution: A Computational Study. *J. Phys. Chem. A* **2009**, *113*, 7548−7555.
(20) Shao, Q.; Fan, Y.; Yang, L.; Gao, Y. Q. From Protein Denaturant to Protectant: Comparative Molecular Dynamics Study of Alcohol/Protein Interactions. *J. Chem. Phys.* **2012**, *136*, 115101.
(21) Smolin, N.; Winter, R. Effect of Temperature, Pressure, and Cosolvents on Structural and Dynamic Properties of the Hydration Shell of SNase: A Molecular Dynamics Computer Simulation Study. *J. Phys. Chem. B* **2008**, *112*, 997−1006.
(22) Mehrnejad, F.; Ghahremanpour, M. M.; Khadem-Maaref, M.; Doustdar, F. Efects of Osmolytes on the Helical Conformation of Model Peptide: Molecular Dynamics Simulation. *J. Chem. Phys.* **2011**, *134*, 035104.
(23) Johnson, M. E.; Malardier-Jugrootd, C.; Head-Gordon, T. Effects of Co-solvents on Peptide Hydration Water Structure and Dynamics. *Phys. Chem. Chem. Phys.* **2010**, *12*, 393−405.
(24) Liu, F.-F.; Ji, L.; Zhang, L.; Dong, X.-Y.; Sun, Y. Molecular Basis for Polyol-Induced Stability Revealed by Molecular Dynamics Simulation. *J. Chem. Phys.* **2010**, *132*, 225103.
(25) Bastiansen, O. Intra-Molecular Hydrogen Bonds in Ethylene Glycol, Glycerol, and Ethylene Chlorohydrin. *Acta Chem. Scand.* **1949**, *3*, 415−421.
(26) Towey, J. J.; Soper, A. K.; Dougan, L. The Structure of Glycerol in the Liquid State: A Neutron Diffraction Study. *Phys. Chem. Chem. Phys.* **2011**, *12*, 9397−9406.
(27) Jahn, D. A.; Akinkunmi, F. O.; Giovambattista, N. Effects of Temperature on the Properties of Glycerol: A Computer Simulation Study of Five Different Force Fields. *J. Phys. Chem. B* **2014**, *118*, 11284−11294.
(28) Towey, J. J.; Soper, A. K.; Dougan, L. What Happens to the Structure of Water in Cryoprotectant Solutions? *Faraday Discuss.* **2013**, *167*, 159−176.
(29) Plimpton, S. Fast Parallel Algorithms for Short-Range Molecular Dynamics. *J. Comput. Phys.* **1995**, *117*, 1−19.
(30) Shinoda, W.; Shiga, M.; Mikami, M. Rapid Estimation of Elastic Constants by Molecular Dynamics Simulation Under Constant Stress. *Phys. Rev. B* **2004**, *69*, 134103.
(31) Hockney, R. W.; Eastwood, J. W. *Computer Simulation Using Particles*; Adam Hilger: New York, 1989.
(32) Berendsen, H. J. C.; Grigera, J. R.; Straatsma, T. P. The Missing Term in Effective Pair Potentials. *J. Phys. Chem.* **1987**, *91*, 6269−6271.
(33) Reiling, S.; Schlenkrich, M.; Brickmann, J. Force Field Parameters for Carbohydrates. *J. Comput. Chem.* **1996**, *17*, 450−468.
(34) Brooks, B. R.; Bruccoleri, R. E.; Olafson, B. D.; States, D. J.; Swaminathan, S.; Karplus, M. CHARMM: A Program for Macromolecular Energy, Minimization, and Dynamics Calculations. *J. Comput. Chem.* **1983**, *4*, 187−217.
(35) Nilsson, L.; Karplus, M. Empirical Energy Functions for Energy Minimizations and Dynamics of Nucleic Acids. *J. Comput. Chem.* **1986**, *7*, 591−616.
(36) Following Egorov et al.,[13] the atomic charge of the central aliphatic hydrogen was set to 0.044*e* to bring the net charge of the glycerol molecule to zero.
(37) Cornell, W. D.; Cieplak, P.; Bayly, C. I.; Gould, I. R.; Merz, K. M.; Ferguson, D. M.; Spellmeyer, D. M.; Fox, T.; Caldwell, J. W.; Kollman, P. A. A Second Generation Force Field for the Simulation of Proteins, Nucleic Acids, and Organic Molecules. *J. Am. Chem. Soc.* **1995**, *117*, 5179−5197.
(38) Jorgensen, W. L.; Maxwell, D. S.; Tirado-Rives, J. Development and Testing of the OPLS All-Atom Force Field on Conformational Energetics and Properties of Organic Liquids. *J. Am. Chem. Soc.* **1996**, *118*, 11225−11236.
(39) Jorgensen, W. L.; Chandrasekhar, J.; Madura, J. D.; Impey, R. W.; Klein, M. L. Comparison of Simple Potential Functions for Simulating Liquid Water. *J. Chem. Phys.* **1983**, *79*, 926−935.
(40) Jorgensen, W. L.; Tirado-Rives, J. J. Potential Energy Functions for Atomic-Level Simulations of Water and Organic and Biomolecular Systems. *Proc. Natl. Acad. Sci. U.S.A.* **2005**, *102*, 6665−6670.
(41) MacKerell, A. D., Jr. Empirical Force Fields for Biological Macromolecules: Overview and Issues. *J. Comput. Chem.* **2004**, *25*, 1584−1604.
(42) More precisely, the water model used in the development of the CHARMM22 FF is the TIP3P model modified for the CHARMM force field; see ref 41.
(43) Abascal, J. L. F.; Vega, C. A General Purpose Model for the Condensed Phases of Water: TIP4P/2005. *J. Chem. Phys.* **2005**, *123*, 234505.
(44) Abascal, J. L. F.; Vega, C. Widom Line and the Liquid-Liquid Critical Point for the TIP4P/2005 Water Model. *J. Chem. Phys.* **2010**, *133*, 234502.
(45) Callen, H. B. *Thermodynamics and Introduction to Thermostatistics*, 2nd ed.; John Wiley & Sons: New York, 1985.
(46) Weng, L.; Chen, C.; Zuo, J.; Li, W. Molecular Dynamics Study of Effects of Temperature and Concentration on Hydrogen-Bond Abilities of Ethylene Glycol and Glycerol: Implications for Cryopreservation. *J. Phys. Chem. A* **2011**, *115*, 4729−4737.
(47) Takamura, K.; Fischer, H.; Morrow, N. R. Physical Properties of Aqueous Glycerol Solutions. *J. Pet. Sci. Eng.* **2012**, *98*−*99*, 50−60.
(48) Marcus, Y. Some Thermodynamic and Structural Aspects of Mixtures of Glycerol with Water. *Phys. Chem. Chem. Phys.* **2000**, *2*, 4891−4896.
(49) Allen, M. P.; Tildesley, D. J. *Computer Simulation of Liquids*; Oxford Science Publications: Oxford, U.K., 1988.
(50) Righetti, M. C.; Salvetti, G.; Tombari, E. Heat Capacity of Glycerol from 298 to 383 K. *Thermochim. Acta* **1998**, *316*, 193−195.
(51) *Physical Properties of Glycerine and its Solutions*; Soap and Detergent Association: New York, 1963.
(52) Angell, C. A.; Shuppert, J.; Tucker, J. C. Anomalous Properties of Supercooled Water. Heat Capacity, Expansivity, and Proton Magnetic Resonance Chemical Shift from 0 to −38°. *J. Chem. Phys.* **1973**, *77*, 3092−3099.
(53) All data sets are fitted using the xmgrace software package, employing the nonlinear regression tool with a weighting factor of $1/y^{3/2}$. This results in improved agreement between the data-set points and the corresponding fitting curve.
(54) Vogel, H. The Law of the Relationship Between Viscosity of Liquids and the Temperature. *Phys. Z.* **1921**, *22*, 645−646.

DOI: 10.1021/acs.jpcb.5b00439
J. Phys. Chem. B 2015, 119, 6250−6261

(55) Tamman, G.; Heese, W. Z. The Dependence of Viscosity on the Temperature of Supercooled Liquids. *Anorg. Allgem. Chem.* **1926**, *156*, 245−257.
(56) Fulcher, G. S. Analysis of Recent Measurements of the Viscosity of Glasses. *J. Comput. Chem.* **1925**, *8*, 339−355.
(57) Chen, B.; Sigmund, E. E.; Halperin, W. P. Stokes-Einstein Relation in Supercooled Aqueous Solutions of Glycerol. *Phys. Rev. Lett.* **2006**, *96*, 145502.
(58) Mills, R. Self-Diffusion in Normal and Heavy Water in the Range 1−45 deg. *J. Chem. Phys.* **1973**, *77*, 685−688.
(59) D'Errico, G.; Ortona, O.; Capuano, F.; Vitagliano, V. Diffusion Coefficients for the Binary System Glycerol + Water at 25°C. A Velocity Correlation Study. *J. Chem. Eng. Data* **2004**, *49*, 1665−1670.
(60) Jorgensen, W. L.; Jenson, C. Temperature Dependence of TIP3P, SPC, and TIP4P water from NPT Monte Carlo Simulations: Seeking Temperatures of Maximum Density. *J. Comput. Chem.* **1998**, *19*, 1179−1186.
(61) Kell, G. S. Density, Thermal Expansivity, and Compressibility of Liquid Water from 0° to 150°. Correlations and Tables for Atmospheric Pressure and Saturation Reviewed and Expressed on 1968 Temperature Scale. *J. Chem. Eng. Data* **1975**, *20*, 97−105.
(62) Adamenko, I. I.; Zelinsky, S. O.; Korolovich, V. V. Thermodynamics Properties of Glycerol-Water Solutions. *Ukr. J. Phys.* **2007**, *52*, 855−859.
(63) Speedy, R. J.; Angell, C. A. Isothermal Compressibility of Supercooled Water and Evidence for a Thermodynamic Singularity at −45°C. *J. Chem. Phys.* **1976**, *65*, 851−858.
(64) With the present total simulation times, we are able to estimate errors in the diffusion coefficients only at high temperatures. The estimated error bars are smaller than the symbol size in Figures 7 and 10.

DOI: 10.1021/acs.jpcb.5b00439
J. Phys. Chem. B 2015, 119, 6250−6261